JMEPEG (2015) 24:3365–3372
DOI: 10.1007/s11665-015-1622-y


1059-9495/$19.00

# Effects of Aging Treatments on the Mechanical Behavior of Ti-15V-3Cr-3Sn-3Al Alloy

*Y.-K. Chou, L.W. Tsay, and C. Chen*

*(Submitted February 25, 2015; in revised form June 17, 2015; published online July 15, 2015)*

**The effect of aging treatments on the mechanical properties and microstructures of Ti-15V-3Cr-3Sn-3Al (Ti-15-3) alloy was evaluated using tensile, notched tensile, and *J*-integral tests. The properties for the one-step aged specimens (371 to 648 °C for 8 h) were compared with those for the two-step aged specimens (one-step aged + 426 °C/24 h). An increase in aging temperature of one-step aging resulted in increased notched tensile strength and fracture toughness of the Ti-15-3 alloy. The second-step aging at 426 °C for 24 h caused various degrees of hardening in the group of double aged specimens. Comparing to the one-step aged specimens, increased notch brittleness and decreased fracture toughness were observed in the two-step aged specimens. For the specimens subjected to aging at 648 °C, the formation of thick α layer at β grain boundaries resulted in lower tensile properties and fracture toughness. The fracture modes of the notch-brittle specimens were strongly affected by the distribution, size, and morphology of the α precipitates.**

**Keywords** *J*-integral, notched tensile strength, Ti-15V-3Cr-3Sn-3Al

## 1. Introduction

Improvement in aircraft performance relies strongly on the advance in materials. Titanium alloys with a high strength-to-weight ratio, corrosion resistance, and fatigue/fracture toughness are widely used in aviation, aerospace, and chemical industries. The demand growth rate for those alloys is expected to increase in the future, mainly because of an increase in the titanium content per aircraft (Ref 1). Beta titanium alloys are an attractive alternative to α-β-Ti alloy because of their increased heat treatability, a wide range of strength-to-weight ratios and cold-forming ability (Ref 2). Amongst beta titanium alloys, Ti-15V-3Cr-3Al-3Sn has been used extensively in airframe applications (Ref 3, 4). Ti-15V-3Cr-3Sn-3Al (Ti-15-3) is used for ducting, clips, brackets, and floor support structures as a replacement for Ti-6Al-4V alloy in the aircraft industry (Ref 4).

Mechanical properties of the Ti-15-3 alloy are known to be affected by its composition (Ref 5, 6) and thermo-mechanical treatments (Ref 7-11). The ultimate tensile strength of this alloy can reach 1562 MPa after cold rolling and aging at 450 °C for 4 h (Ref 9). Following the thermo-mechanical treatments of the Ti-15-3 alloy, a good balance is achieved between high strength and ductility as the results of a much finer and uniform α + β structure (Ref 10, 11). With an increase in aging temperature, the volume fraction of the α phase decreases and the size of the secondary α increases, which account for lowered strength and improved ductility of a newly developed β-Ti alloy (Ref 12). The microstructures also have shown a great influence on the fatigue properties and fatigue crack-growth behavior of Ti-15-3 alloy (Ref 13). For a specimen in the solution-treated condition, the fatigue crack tends to follow the slip bands in a given crystallographic plane. By contrast, crack propagation occurs on non-crystallographic plane and is strongly related to the configuration of α platelets (Ref 13). Moreover, coarse α platelets in over-aged specimens are beneficial to fatigue crack-growth resistance in the Ti-15-3 alloy as compared with the under- and peak-aged specimens (Ref 14).

It has been reported that an increase in tensile strength of the Ti-15-3 alloy is accompanied by a decrease in ductility and fracture toughness (Ref 15). In previous studies, the influence of microstructures on the notch brittleness of titanium alloys and welds has been investigated by using notched tensile specimen (Ref 16-19). With the presence of sharp notches, the induced embrittlement of the specimens can be reduced through proper heat-treating processes. In this work, two-step as well as one-step aging treatments of Ti-15-3 alloy were performed to compare the mechanical properties of the specimens using two process routes. The notched tensile strength and fracture toughness of the aged Ti-15-3 specimens were determined to evaluate the susceptibility of the specimens to notch brittleness. The results of the tests were related to the microstructures and fracture features of the alloy.

## 2. Experimental Procedures

### 2.1 Materials

A 3.0-mm-thick sheet of Ti-15-3 alloy was used in this work. The chemical composition of the experimental material in wt.% was 3.05 Al, 2.92 Cr, 2.99 Sn, 15.1 V, 0.071 Fe, 0.12 O, 0.016 C, 0.014 N, and 0.021 S, with a balance of titanium. The as-received material was subjected to solution-annealed treatment at 800 °C for 0.5 h, followed by Ar-assisted cooling to room temperature. The solution-treated specimens were then

**Y.-K. Chou** and **C. Chen**, Department of Materials Science and Engineering, National Taiwan University, Taipei 106, Taiwan, ROC; and **L.W. Tsay**, Institute of Materials Science and Engineering, National Taiwan Ocean University, Keelung 202, Taiwan, ROC. Contact e-mail: b0186@mail.ntou.edu.tw.

either one-step or two-step aged in a vacuum furnace. The one-step aging treatments were performed at various temperatures from 317 to 648 °C for 8 h, followed by Ar-assisted cooling to room temperature. The one-step aged specimens were identified by three-digital numbers prefixed with a capital letter A to indicate the aging temperature. Thus, the designation of A482 represented the specimen aged at 482 °C for 8 h. A plateau of the hardness curve was obtained for the specimens subjected to prolonged aging at 426 °C for 24 h. Therefore, further hardening of the one-step aged specimens could be achieved by a second-step aging, which was kept at 426 °C for 24 h. For the specimens subjected to two-step (or double) aging treatments, a capital letter D was added before the one-step aging temperature, e.g., the D593 specimen indicated that the one-step aging was performed at 593 °C for 8 h, followed by a second aging at 426 °C for 24 h.

### 2.2 Hardness and Tensile Tests

A Vickers microhardness tester was used to measure the specimen hardness under a load of 300 g for 10 s. At least 5 indentations were performed to measure hardness of variously aged specimens. In accordance with the ASTM E8/8M-13a standard (Ref 20), a smooth tensile specimen with a gage length of 25 mm, width of 6.25 mm, and thickness of 3.0 mm was used to determine tensile properties. The tensile tests were performed at room temperature at a constant cross-head speed of 1.0 mm/min.

### 2.3 Notched Tensile Test

A double-edged notched specimen, which comprised of a sharp notch with a tip radius of approximately 100 μm and a notch depth of 7.0 mm, was used in this study (Ref 16). The notched strength ratio (NSR) of a specimen was defined as the notched tensile strength (NTS) divided by its ultimate tensile strength (UTS), which was used as an index to indicate the notch brittleness of the specimen in the presence of a sharp notch. For NSR considerably smaller than 1, it meant high notch brittleness of the specimen. Notched tensile tests were performed at a constant cross-head-displacement rate of 1.0 mm/min at room temperature.

### 2.4 Fracture Toughness Test

According to the ASTM E399-08 standard (Ref 21) to measure the plain strain fracture toughness, the specimen thickness requires to exceed a minimum value, which is dependent on the yield strength of the alloy. Moreover, the J-R curve is a reliable fracture toughness measurement for elastic-plastic materials. In accordance with the ASTM E1737-96 standard (Ref 22), a compact tension (CT) specimen with 3.0-mm pre-crack was employed to determine the *J*-R (*J*-integral versus crack extension) curves of the double aged specimens by using single specimen technique. All the mechanical data were the results of duplicated tests with 3 samples.

### 2.5 Microstructural Observations

After metallographic preparations, all the specimens were etched by the solution containing 1% HF + 1.5% $HNO_3$ + 97.5% $H_2O$, then examined by FEI Nova 450 scanning electron microscope (SEM). For detailed microstructural observations, thin foil specimens were prepared by a twin-jet-polisher, then examined by a Joel 2000 EX transmission electron microscope (TEM). A mixture solution of 6% $HClO_4$ + 34% $C_4H_9OH$ + 60% $CH_3OH$ was used for the electrochemically polishing of TEM sample at −20 °C. The macro- and detailed fracture features of various specimens were also inspected by SEM.

## 3. Results

### 3.1 Microhardness Measurements

Figure 1 shows the variation of microhardness in Ti-15-3 alloy after the one-step or two-step aging treatments. The hardness of Ti-15-3 alloy in the solution-annealed condition was approximately Hv 274. For the one-step aged specimens, a great variation in hardness was found. Among the one-step aged specimens, the A426 specimen exhibited a peak hardness of Hv 428. With an increase in aging temperature above 482 °C, a gradual drop in hardness was observed. These results indicated clearly that one-step aging at 426 °C for 8 h could effectively harden the Ti-15-3 alloy for practical applications. In the case of the double aged specimens, the D317, D371, and D426 specimens possessed somewhat similar hardness of approximately Hv 450. This reflected the fact that the double aged specimens initially aged at 317 and 371 °C could be hardened further in the second-step aging (426 °C/24 h). Therefore, the under-aged conditions in the first aging (A317 and A371) had little influence on the hardness of the corresponding double aged specimens (D317 and D371). Besides, the A538 (Hv 376) and A593 (Hv 343) specimens had similar hardness to the D538 (Hv 383) and D593 (Hv 346) specimens, respectively. The results implied that little or no further precipitation of α in such specimens during the second-step aging (426 °C for 24 h). Interestingly, the D648 specimen exhibited an obviously higher hardness (Hv338) than the A648 specimen (Hv290). It was deduced the precipitation of fine α in the matrix of D648 specimen during the second-step aging was responsible for the increase in hardness (discussed latter in the text).

### 3.2 Microstructural Observations

Figure 2 displays the microstructures of various specimens. The optical microstructures of the solution-annealed Ti-15-3

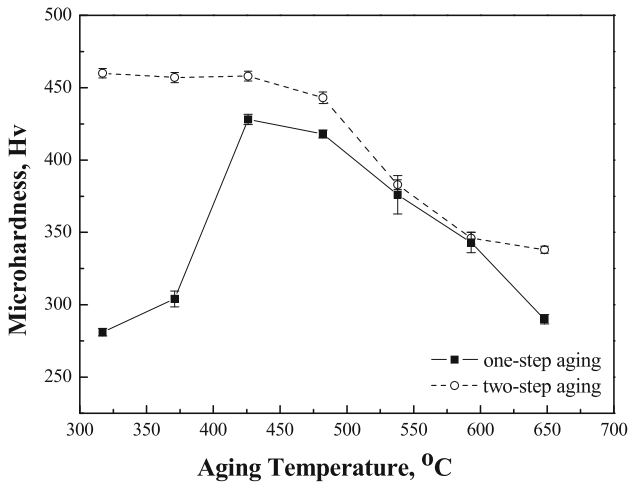


**Fig. 1** The variation of microhardness in Ti-15-3 alloy after one-step or two-step (double) aging treatments

alloy revealed that equiaxed β grains (about 68 μm grain size) without any observable precipitates (Fig. 2a). Aging treatments caused the precipitation of α phase in different sizes and extents, resulting in distinct degrees of age-hardening (Ref 23). Extremely fine α aggregates were observed to be sparsely distributed in the matrix of A371 specimen (Ref 23). Needle-like fine α precipitated uniformly in the β matrix of the A426 specimen, which could account for the highest hardness among the one-step aged specimens (Ref 23). For the two-step aged specimens with similar microstructures, e.g., the D426, D371, and D317 specimens, their hardness values were alike. Fine interlocking α precipitates in the basket-weave form were observed in the SEM micrographs of the D371 specimen (Fig. 2b). To further inspect the morphology of interlocked α, TEM examinations were carried out to confirm the fine needle-like α in the D426, D371, and D317 specimens (Fig. 2c). It should be noted that α precipitates of different sizes were observed in all the aged specimens. Therefore, it was difficult to distinguish the α precipitates formed in the second step of the aging treatment from those formed in the first step. However, some α precipitates must have been generated in the second step, which resulted in a slight increase in the hardness relative to the one-step aged specimens.

It is reported (Ref 12) a decrease in volume fraction and coarsening of α phase of a newly developed β-Ti alloy with increasing aging temperature account for the lowered strength and improved ductility. In the current study, the coarsening of α precipitates was responsible for a decrease in hardness of the A482 and D482 specimens relative to that of the A426 and D426 specimens. Aging at and above 538 °C resulted in an obvious increase in α size in the matrix as well as at the grain boundaries (Fig. 2d-h), regardless of the aging routes. However, there is a great difference in intragranular α size between the specimens aged at 538 and 593 °C. Both the A538 and D538 specimens comprised relatively fine α distributed in the matrix (Fig. 2d). For the specimens aged at 593 °C, a significant coarsening in α size occurred, as shown in (Fig. 2e). It was found that the A593 and D593 specimens had nearly identical hardness. The size of α platelets in both specimens was similar after extensive examinations. The difference in size of α platelets in different grains could be attributed mainly to the orientation effect ((Fig. 2e and f). Interestingly, extremely short and needle-like α precipitates, as indicated by arrows, were found to be dispersed in the β matrix of the D648 specimen (Fig. 2g). In contrast, fine α precipitates were hardly found in the A648 and other specimens (Fig. 2h). It was evident the difference in hardness between the A648 and D648 specimens was associated with the formation of extra needle-like α precipitates in the D648 specimen.

### 3.3 Tensile and Notched Tensile Tests

Figure 3 displays the variations in UTS and NTS with aging temperature after one-step and two-step aging treatments. In general, the effect of aging treatment on the change in the UTS of the specimen was in the same trend as the variation in hardness, as shown in Fig. 1, i.e., the higher the hardness the greater the UTS of the specimen. However, the NTS of the aged specimen could be much lower than its UTS, especially for those highly age-hardened specimens, irrespective of the aging routes. The results indicated that the A538 specimen had the highest NTS among the one-step aged specimens (Fig. 3a). Aging at 426 °C in the second step of the aging treatment caused an appreciable increase in UTS of the D371 specimen, but played a minor role on the UTS of D538 and D593 specimens (Fig. 3b). The UTS of D538 and D593 specimens was therefore similar to those of the A538 and A593 specimens, accordingly. It is worth mentioning that the A538 specimen comprised moderate UTS (1225 MPa) and high NTS (1449 MPa) compared with the other one-step aged specimens. Moreover, the peak NTS among the double aged specimens was observed in the D593 specimen.

Figure 4 shows the specimen elongation and NSR versus aging temperature after one-step and two-step aging treatments. The results indicate those specimens composed of low elongation were associated with low NSR or high notch brittleness, regardless of aging routes. It revealed that the ductility had a predominant effect on the NSR or notch brittleness of the specimens. In the case of one-step aged specimens (Fig. 4a), the NSRs of A538, A593, and A648 were greater than one, showing a better resistance to crack growth in the presence of a sharp notch. Besides, a drop in NSR was found in A648 specimen. For the double aged specimens (Fig. 4b), only the D593 specimens showed an NSR greater than 1. The D648 specimen showed a poor elongation (6%) and low NSR (0.87) relative to the D538 and D593 specimens. Moreover, the elongation of the D648 (6%) specimen was much lower than that of the A648 specimen (20%).

### 3.4 Fracture Toughness

The $J_{0.2}$ value, the intersection of the $J$-R curve and 0.2-mm offset line, was used as an index to characterize the fracture toughness of the Ti-15-3 alloy. The $J$-R curves of the double aged specimens are shown in Fig. 5, and the measured $J_{0.2}$ values of the D426, D482, D538, D593, and D648 specimens were 9.5, 15.0, 27.0, 65.0, and 36.0, respectively. The fracture toughness increased with aging temperature up to 593 °C and then decreased with a further increase in aging temperature. For the hardened specimens, e.g., the D426 and D482 specimens, the $J_{0.2}$ values were considerably lower than the D538, D593, and D648 specimens. Additionally, the D593 specimen showed the highest NTS, $J_{0.2}$ values and tensile ductility among the two-step aged specimens. The combination of moderate strength and ductility appears to correspond to a high NSR and fracture toughness.

### 3.5 Fracture Appearance

Figure 6 displays the typical fracture appearance of various specimens after various tests. For the A371, A426, D371, and D426 specimens with low tensile ductility or a low NSR (high notch brittleness), the macro-fracture appearance of those specimens exhibited wide flat fracture (FF) regions after tensile tests (Fig. 6a). By contrast, for the specimens with an NSR greater than 1, such as the A538, A593, and D593 specimens, shear fracture (SF) instead of wide flat fracture was observed in the specimen (Fig. 6b). In particular, a specimen showed the same fracture feature irrespective of whether the sharp notch was present. In the fracture toughness test, the specimens with low toughness comprised a flat crack-growth region (Fig. 6c). By contrast, shear fracture was seen after crack growth into the D593 specimen (Fig. 6d), reflecting the dissipation of deformation energy before fracture.

Figure 7 shows the detailed fracture features of the tested specimens examined by SEM. These highly age-hardened

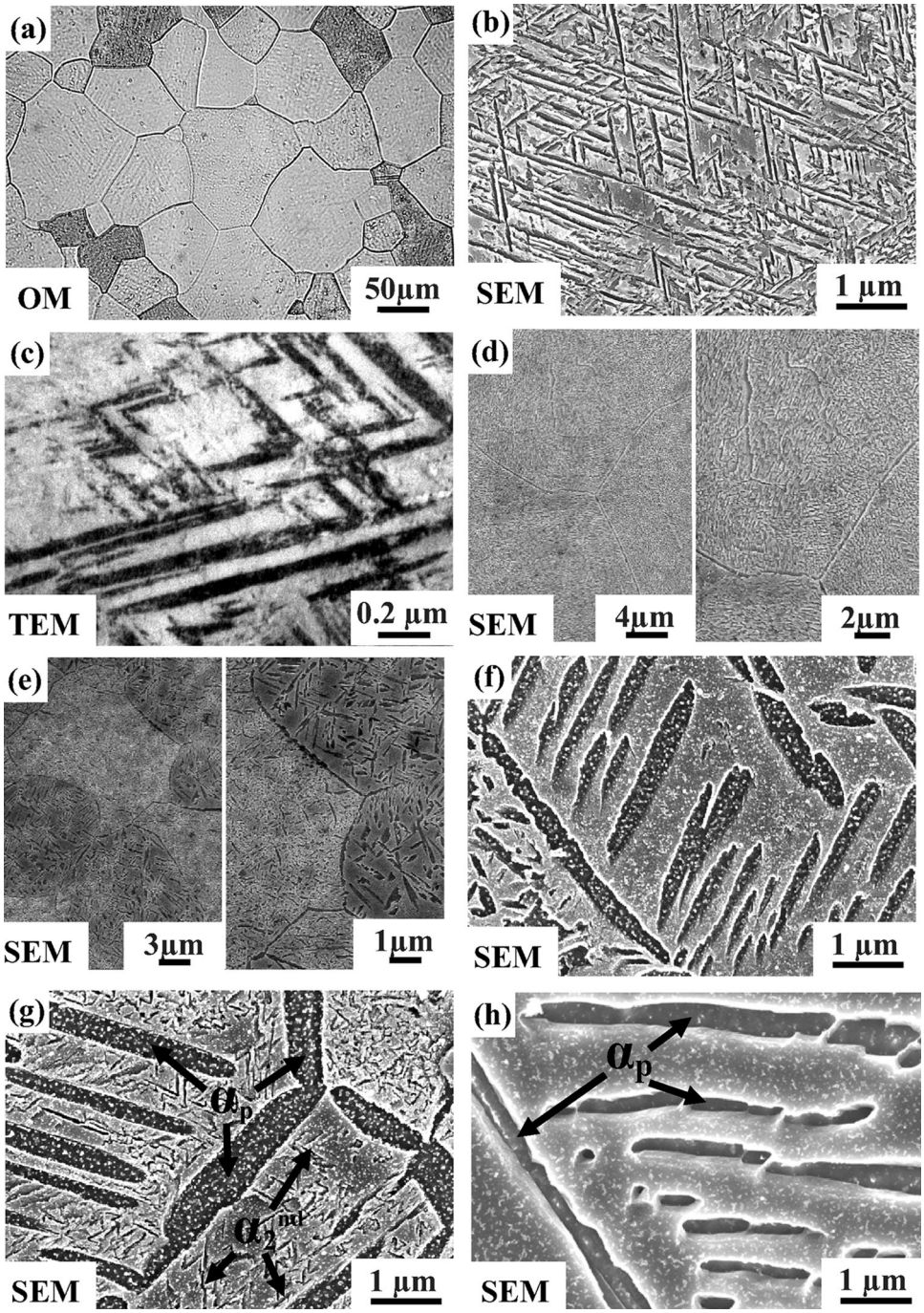


**Fig. 2** The microstructures of the (a) solution-annealed, (b) D371, (c) D426, (d) A538, (e) A593, (f) D593, (g) D648, and (h) A648 specimens

specimens (A426, D371, and D426) with a low NSR displayed quasi-cleavage fracture mixed with shallow dimples after tensile tests (Fig. 7a). The A371 specimen also showed a wide cleavage-like fracture (Fig. 7b), which accounted for the low ductility of the specimen. With increasing aging temperature, mainly dimple fracture instead of quasi-cleavage was found in the over-aged specimens (Fig. 7c). The formation of large dimples was associated with the presence of coarse α platelets in the over-aged specimens. As mentioned previously, a sharp drop in NTS was seen in the A648 and D648 specimens relative to the A593 and D593 specimens, accordingly. The decrease in the UTS/NTS of the A648 and D648 specimens was attributed to the occurrence of intergranular shear separations (Fig. 7d), which were seen more frequently in the D648 specimens. It was thought that the ease of shear fracture along the grain boundaries of the D648 specimens was responsible for the reduced strength and ductility. Furthermore, the fracture morphology of two-step aged specimens after fracture toughness test (Fig. 7(e and f) showed fracture features identical to those of the notched tensile specimens.

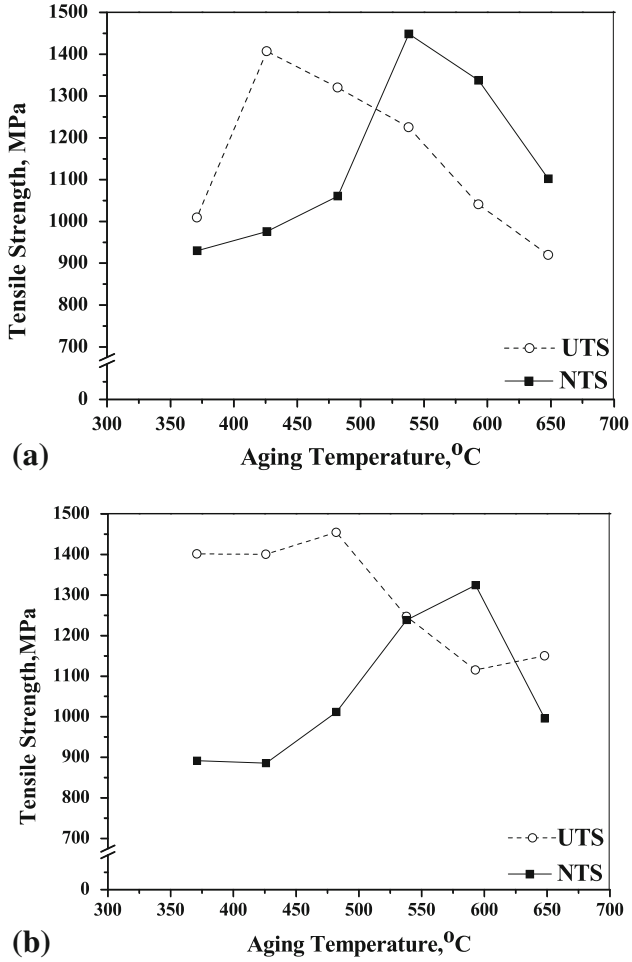


**Fig. 3** The variation in ultimate tensile strength (UTS) and notched tensile strength (NTS) with aging temperatures after (a) one-step and (b) two-step aging treatments

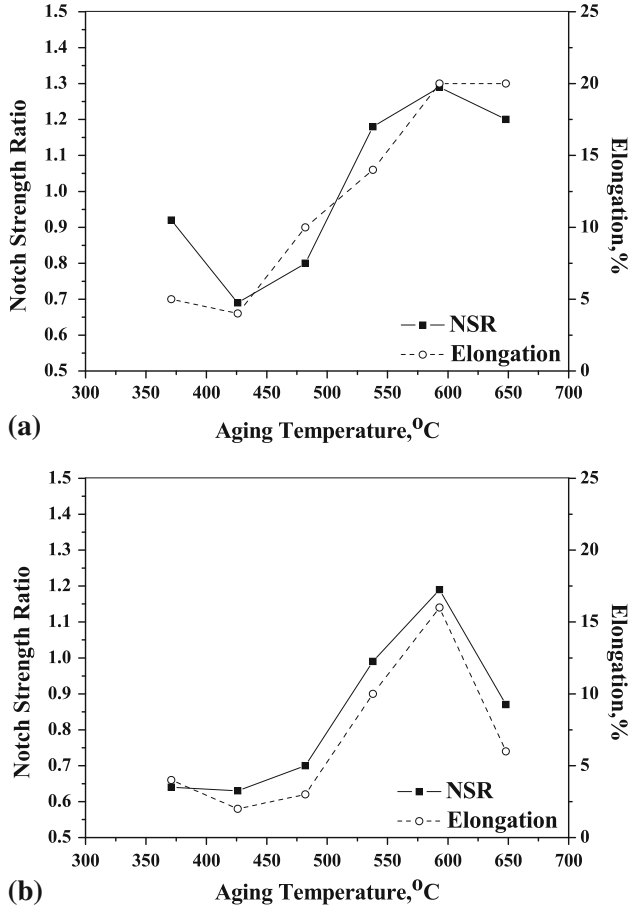


**Fig. 4** The notch strength ratio (NSR) and elongation vs. aging temperatures for the (a) one-step and (b) two-step aged specimens

## 4. Discussion

Various amounts of fine α precipitates led to a different degrees of age-hardening in Ti-15-3 alloy. The results indicated an increase in hardness of the double aged specimens was accompanied with a decrease in their ductility and toughness as compared with the one-step aged specimens. Regardless of aging routes, the significantly hardened (D426, D371, A426) or severely over-aged (D648) specimens were notch sensitive and low ductility. The β-trans temperature of the Ti-15-3 alloy was estimated approximately 760 °C. With an increase in aging temperature up to 426 °C, the increased amount of α precipitates caused age-hardening in the one-step aged specimens. Under a fixed aging time, the precipitation of α-Ti from the β matrix is temperature dependent. As a result, there is an optima temperature that the precipitation of α will be at the greatest amount during aging. Above a certain aging temperature, the coarsening of α precipitates together with a decrease in α content occurred simultaneously. It was deduced a greater fraction of β was retained in the A648 specimen, as compared

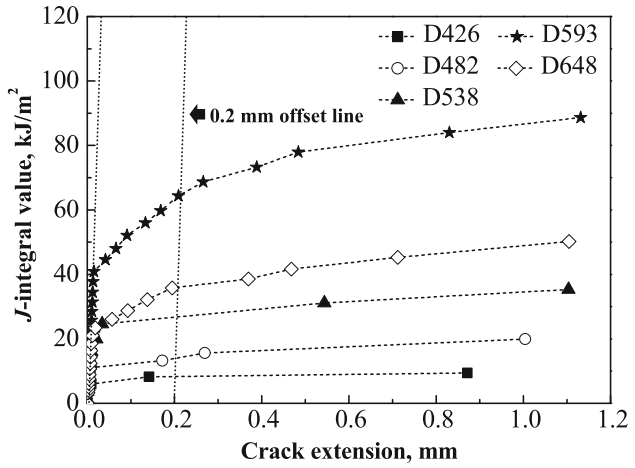


**Fig. 5** The J-integral plotted against crack extension curves of the two-step aged specimens

with that in the other one-step aged specimens. After the second-step aging at 426 °C/24 h, the newly formed α precipitates in the D648 specimen were much smaller in size

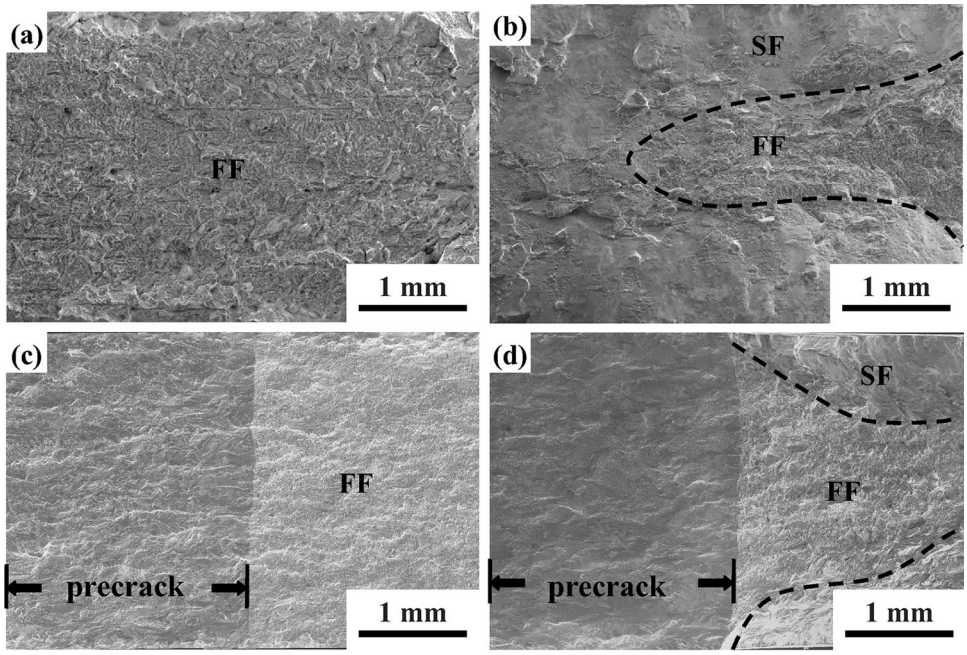


**Fig. 6** The macro-fracture appearance of the (a) D426 and (b) D593 specimens after notched tensile tests; (c) D426 and (d) D593 specimens after fracture toughness tests

(Fig. 2e), which could not be observed in other two-step aged specimens. Such fine α precipitates present in the D648 specimen were responsible for the increased hardness, as compared to the A648 specimen. Because of the further strengthening of the matrix by fine α precipitates, the straining of the D648 specimen became more localized around grain boundaries. Therefore, the ease of separation along grain boundaries resulted in the low ductility and low NSR (high notch brittleness) of the D648 specimen.

It was noticed that the age-hardened specimens, such as the D371, D426, and A426 specimens, also showed poor toughness, low ductility, and NSR, as shown in Fig. 4 and 5. The effective strengthening of the specimens by fine needle-like α precipitates impeded the dislocation motion and led to the limited ductility of these specimens. An extensive cleavage-like fracture was observed in all of the specimens after different tests. As mentioned previously, the D648 specimen with low NSR and ductility exhibited intergranular shear along with dimple fractures; a completely different type of fracture feature from that of the specimens which were significantly hardened. It was concluded a thin α layer formed at grain boundaries of the specimens aged at less than 538 °C played a minor role on the fracture of Ti-15-3 alloy. If the α layer at grain boundaries was sufficiently thick, the shearing fracture along weak α layer located at the boundaries led to premature failure. Thus, thick α layer was harmful to mechanical properties just like in the A648 and D648 specimens. Therefore, the inherent microstructures played a major role on the notch brittleness of the Ti-15-3 alloy. It was concluded the reduction in strength by increasing aging temperature would not always accompany with an increase in ductility, NSR, and toughness of the Ti-15-3 alloy. The maximum toughness/NTS could be achieved by choosing a suitable combination of tensile strength and ductility, which was associated with optimum microstructures.

## 5. Summary

Regardless of the aging temperature of the first step in the two-step aging process, a second-step aging at 426 °C/24 h further increased the hardness of the one-step aged specimens but to different degrees. The limited precipitation of α during the second aging caused a minor increase in hardness of the specimens when the first-step aging temperature was not less than 538 °C. The low ductility of the A426, D371, and D426 specimens was responsible for the high sensitivity to notch brittleness, low NSR, and fracture toughness of the specimens. An extensive cleavage-like fracture was the dominant fracture feature in the specimens which were significantly hardened (A426, D371, and D426). In contrast, the formation of thick α layer at grain boundaries along with extra fine precipitates inter-dispersed in the matrix of the D648 specimen caused localized deformation around grain boundaries during straining. The ease of shearing fracture along weak α layer located at the boundaries resulted in degraded mechanical properties of the A648 and D648 specimen. The results indicated that the inherent microstructures played a major role in determining the notch brittleness of the Ti-15-3 alloy. The maximum fracture toughness/NTS of the specimen could be achieved by a suitable combination of high tensile strength and ductility for the specimen aged at 593 °C (D593 specimen) in the group of two-step aged specimens.

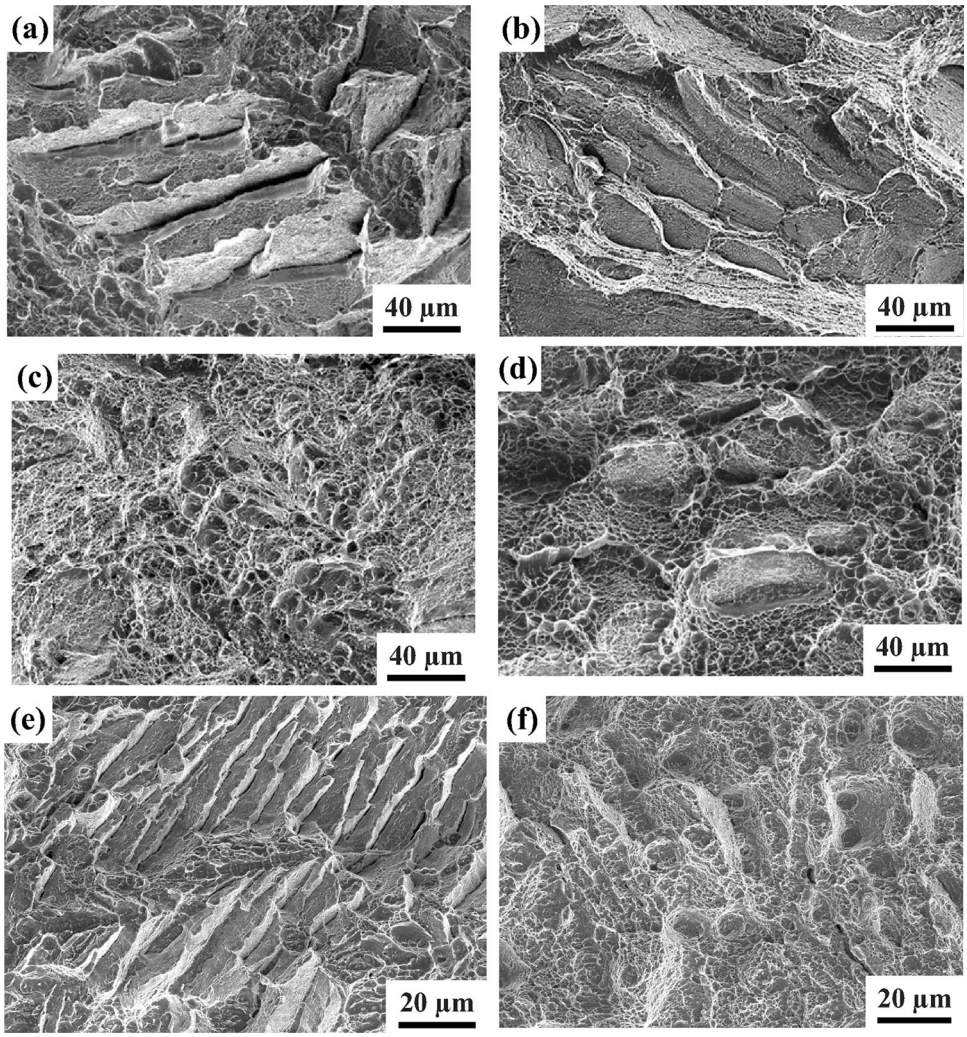


**Fig. 7** The typical fracture appearance of the (a) D426, (b) A371, (c) A593, and (d) D648 specimens after notched tensile tests; (e) D426 and (f) D593 specimens after fracture toughness tests

## Acknowledgment

The authors gratefully acknowledge the support of this study by the National Science Council, Republic of China (NSC100-2221-E-019-031).

## References

1. C.X. Cui, B.M. Hu, L.C. Zhao, and S.J. Liu, Titanium Alloy Production Technology, Market Prospects and Industry Development, *Mater. Des.*, 2011, **32**, p 1684–1691
2. J.C. Fanning and S.P. Fox, Recent Developments in Metastable β Strip Alloys, *J. Mater. Eng. Perform.*, 2005, **14**, p 703–708
3. R.R. Boyer, Attribute, Characteristics, and Application of Titanium and Its Alloys, *J. Met.*, 2010, **62**, p 21–26
4. R.R. Boyer and R.D. Briggs, The Use of Beta Titanium Alloys in the Aerospace Industry, *J. Mater. Eng. Perform.*, 2013, **22**, p 2916–2920
5. J. Ma and Q. Wang, Aging Characterization and Application of Ti-15-3 Alloy, *Mater. Sci. Eng. A*, 1998, **243**, p 150–154
6. J.D. Prado, X. Song, D. Hu, and X.H. Wu, The Influence of Oxygen and Carbon-Content on Aging of Ti-15-3, *J. Mater. Eng. Perform.*, 2005, **14**, p 728–734
7. F. Furuhara, T. Maki, and T. Makino, Microstructure Control by Thermo-Mechanical Processing in β-Ti-15-3 Alloy, *J. Mater. Proc. Technol.*, 2001, **117**, p 318–323
8. M. Okada, Strengthening of Ti-15V-3Cr-3Sn-3Al by Thermo-Mechanical Treatments, *ISIJ*, 1991, **31**, p 834–839
9. Q. Guo, Q. Wang, D.L. Sun, X.L. Han, and G.H. Wu, Formation of Nanostructure and Mechanical Properties of Cold-Rolled Ti-15V-3Sn-3Al-3Cr Alloy, *Mater. Sci. Eng. A*, 2010, **527**, p 4229–4232
10. O.M. Ivasishin, P.E. Markovsky, Y.V. Matviychuk, S.L. Semiatin, C.H. Ward, and S. Fox, A Comparative Study of the Mechanical Properties of High-Strength β-Titanium Alloys, *J. Alloy Compd.*, 2008, **457**, p 296–309
11. O.M. Ivasishin, P.E. Markovsky, S.L. Semiatin, and C.H. Ward, Aging Response of Coarse-and Fine-Grained β Titanium Alloys, *Mats. Sci. Eng. A*, 2005, **405**, p 296–305
12. Z.X. Du, S.L. Xiao, L.U. Xu, J. Tian, F.T. Kong, and Y.Y. Chen, Effect of Heat Treatment on Microstructure and Mechanical Properties of a New β High Strength Titanium Alloy, *Mater. Des.*, 2014, **55**, p 183–190
13. Z.N. Ismarrubie, A. Ali, T. Satake, and M. Sugano, Influence of Microstructures on Fatigue Damage Mechanisms in Ti-15-3 Alloy, *Mater. Des.*, 2011, **32**, p 1456–1461
14. L.W. Tsay, S.T. Chang, and C. Chen, Fatigue Crack Growth Characteristics of Ti-15V-3Cr-3Sn-3Al Alloy with Variously Aged Conditions, *Mater. Trans. JIM*, 2013, **54**, p 326–331

15. Y. Kawabe and S. Muneki, Strengthening and Toughing of Titanium Alloys, *ISIJ*, 1991, **31**, p 785–791
16. W.C. Chung, L.W. Tsay, and C. Chen, Microstructure and Notch Properties of Heat-Treated Ti-4.5Al-3V-2Mo-2Fe Laser Welds, *Mater. Trans. JIM*, 2009, **50**, p 544–550
17. L.W. Tsay, Y.C. Jian, and C. Chen, The Effect of Preheating on Notch Fracture of SP-700 Laser Welds, *Mater. Trans. JIM*, 2009, **50**, p 2396–2402
18. L.W. Tsay, Y.C. Jian, and C. Chen, Notched Tensile Fracture of Ti-6Al-6V-2Sn Laser Welds at Elevated Temperatures, *ISIJ*, 2010, **50**, p 128–132
19. L.W. Tsay, Y.C. Jian, and C. Chen, Notched Tensile Fracture of Ti-4-5Al-3V-2Fe-2Mo Laser Welds at Elevated temperatures, *Mater. Chem. Phys.*, 2010, **120**, p 715–721
20. ASTM Standard test methods for tension testing of metallic materials, ASTM E8/8M-13a
21. ASTM Standard test methods for linear-elastic plane-strain fracture toughness $K_{IC}$ of metallic materials, ASTM E 399-08
22. ASTM Standard test method for J-Integral characterization of fracture toughness, ASTM E1737-96
23. H.H. Hsu, Y.C. Wu, and L.W. Tsay, Notched Tensile Fracture of Ti-15V-3Cr-3Sn-3Al Alloy, *Mater. Sci. Eng. A*, 2012, **545**, p 20–25